A new high-resolution sea surface temperature blended analysis

A NEW HIGH-RESOLUTION SEA SURFACE TEMPERATURE BLENDED ANALYSIS

Eileen Maturi, Andy Harris, Jonathan Mittaz, John Sapper, Gary Wick, Xiaofang Zhu, Prasanjit Dash, and Prabhat Koner

NOAA's new operational analysis combines polar-orbiting and geostationary data to provide daily global fields of sea surface temperature on a 0.05° (~5 km) grid for a range of applications in climate, ecosystems, weather, and mesoscale oceanography.

Sea surface temperature (SST) is a key geophysical parameter that influences many physical and biological Earth system processes that occur on a wide range of time and space scales. Consequently, there is considerable demand for information on SST products with even higher spatial resolution as input for applications—in particular, gap-free SST analyses for the global ocean. Now quite a number of centers generate such products (e.g., see Martin et al. 2012; Dash et al. 2012). All such analyses utilize SST observations from satellites as their main input since the sparsity of traditional in situ sources (ship, buoy, etc.) do not furnish the necessary coverage (see Fig. 7 later). Deciding on appropriate methods for analyzing such data has been the subject of research for more than two decades (e.g., Reynolds and Smith 1994) and the requirement for higher spatial resolution (cf. Liu et al. 2014), along with increased availability of sources of satellite SST data (Reynolds et al. 2007), has necessitated an evolution in approach. Data from many spaceborne sensors may now be combined to produce the final result and the number and density of observations is now significantly larger in comparison to the situation prior to the millennium.

The increase in data volume and number of satellite sources create certain challenges, especially when coupled with the requirement for high resolution. Each data type needs to be treated carefully to avoid injecting significant errors into the final result. If this can be accomplished, the availability of substantial volumes of high-resolution SST data offers the prospect of overcoming the traditional trade-off between feature resolution and pixel noise (Reynolds

AFFILIATIONS: Maturi—NOAA/NESDIS/STAR, College Park, Maryland; Harris and Koner—NOAA/NESDIS/STAR, and CICS, University of Maryland, College Park, College Park, Maryland; Mittaz—University of Reading, Reading, United Kingdom; Sapper—NOAA/NESDIS/OSPO, College Park, Maryland; Wick—NOAA/OAR/ESRL, Boulder, Colorado; Zhu—NOAA/NESDIS/STAR, College Park, and Global Science and Technology, Inc., Greenbelt, Maryland; Dash—NOAA/NESDIS/STAR, College Park, Maryland, and CIRA, Colorado State University, Boulder, Colorado
CORRESPONDING AUTHOR: Eileen Maturi, eileen.maturi@noaa.gov

The abstract for this article can be found in this issue, following the table of contents.
DOI:10.1175/BAMS-D-15-00002.1

In final form 17 August 2016

et al. 2007). Exploring ways to realize this potential was the major theme of a workshop hosted at the National Oceanic and Atmospheric Administration (NOAA)/National Environmental Satellite, Data, and Information Service (NESDIS) in 2001 (Harris and Maturi 2003), which looked at particular ways to exploit the best characteristics of SST observations from geostationary and polar-orbiting thermal infrared sensors in a combined high-resolution analysis. The work presented here is a realization of at least some of the ideas presented during that workshop.

INPUT DATA. One of the key motivations for developing the new analysis was the desire to maximize the strengths of each input satellite dataset in the production of a high-resolution global SST field.

Polar-orbiting sensors, such as the Advanced Very High Resolution Radiometer (AVHRR) carried on board low-Earth-orbit meteorological satellites [the NOAA and Meteorological Operational (MetOp) platforms], typically image each geographic location twice per day (once in daylight and again at night). MetOp AVHRRs obtain a spatial resolution on the order of 1 km, although the older-generation NOAA platforms lack the ability to record a full orbit at maximum resolution. Thus a subsampled and averaged pixel with effective resolution of ~4 km is available. Recently, data from the NOAA platforms have been superseded by SST data retrieved from the Visible and Infrared Imaging Radiometer Suite (VIIRS) on the *Suomi National Polar-Orbiting Partnership* (*SNPP*) platform, providing global observations at <1-km resolution, again approximately twice per day. The major advantages of such data are the high resolution and retrieval accuracy. Since accurate SSTs cannot be obtained from thermal infrared data in the presence of cloud, observations are confined to areas that have been screened for cloud by automated algorithms (e.g., Merchant et al. 2005).

In contrast to the polar-orbiting sensors, geostationary sensors observe the same geographic location many times per day—up to 96 in the case of the Spinning Enhanced Visible and Infrared Imager (SEVIRI) carried on board the Meteosat Second Generation (MSG) platforms, but with a somewhat reduced spatial resolution and accuracy. While the pixel size remains in the vicinity of 3–4 km at nadir, recent algorithm advances mean that observation accuracy now approaches that of polar-orbiting sensors (Maturi et al. 2008; Merchant et al. 2009, 2013; Koner et al. 2015). The main advantage of geostationary SST data is the observation frequency, which permits greater cloud-free coverage on a daily basis (see Fig. 2 later). The characteristics of each data input are briefly summarized below.

Polar-orbiter instrument data. As already mentioned, the polar-orbiter data come from infrared imaging instruments carried on board the European Organisation for the Exploitation of Meteorological Satellites (EUMETSAT)-operated MetOp series (AVHRR) and the *Suomi NPP* platform (VIIRS).

AVHRR. The venerable AVHRR instrument has been carried on board operational NOAA meteorological satellites for more than three decades. The latest version of the instrument, AVHRR/3, has been carried on all operational NOAA polar-orbiting platforms since *NOAA-15*, launched in 1998. To obtain more than the twice-per-day coverage available from a single platform, NOAA maintained one platform in a "morning" sun-synchronous orbit (equator crossing between ~0800 and ~1000 local time) and a second one in an "afternoon" orbit (between ~1330 and ~1530 local time). Both orbits were sun synchronous, although the exact time of equator crossing depended on both the initial orbit and orbital drift during the satellite lifetime. In 2006, under a cooperative agreement, EUMETSAT launched *MetOp-A* carrying AVHRR/3 in a 0930 local time orbit, and NOAA ceased to launch platforms in a morning orbit. As mentioned previously, the data storage on board the older NOAA platforms was insufficient for a full orbit's worth of AVHRR data to be recorded at native sensor resolution (~1 km); thus, only the subsampled and averaged global area coverage (GAC) format (effective resolution ~4 km) was available for processing to SST for the global ocean. In contrast, the more modern design of the MetOp platform allows recording of the AVHRR data at full resolution. Improved data dissemination capabilities allow for timely access to these datasets.

VIIRS. NOAA's current operational imager is now the VIIRS instrument carried on board the *SNPP* platform. It is NOAA's primary afternoon operational meteorological platform. The VIIRS instrument is a modern radiometer design with 16 channels, 5 of which have significant sensitivity to SST (cf. 3 for the AVHRR). In addition, the sensor resolution is ~750 m at nadir and full resolution is available for the whole globe.

Geostationary instrument data. Geostationary Operational Environmental Satellite (GOES) Imager. NOAA operates two three-axis stabilized geostationary platforms centered at 75° and 135°W. Each carries an SST-capable imager with five channels and a pixel size of approximately 4 km at nadir in the thermal infrared.

It scans north and south sectors at 30-min intervals with a full-disk image taken once every 3 hours. The three-axis stabilization allows a longer dwell time per pixel than the previous generation spin–scan design, significantly improving radiometric noise, and therefore improving SST retrieval accuracy. One drawback is the harsh thermal environment where the instrument experiences a temperature difference of ~40 K between day and night. This effect leads to a residual cycle in calibration bias of up to ~0.7 K (Yu et al. 2013; Mittaz et al. 2013).

Multifunctional Transport Satellite (MTSAT) Imager. The MTSAT Imager is a similar design to the GOES Imager with concomitant strengths and weaknesses. NOAA receives MTSAT radiance data from the Australian Bureau of Meteorology (BoM), limited to one scene per hour owing to bandwidth constraints. There have been two functioning MTSAT platforms. *MTSAT-1R* was launched in 2005 and positioned at 140°E, while *MTSAT-2* was launched in 2010 at 145°E. *MTSAT-2* data production ceased in December 2015 and was replaced by the recently launched *Himawari-8* as the operational geostationary platform for that region of the globe. It carries the modern Advanced Himawari Imager (AHI) instrument, with a more rapid image cycle (full disk every 10 min), higher spatial resolution (2 km at nadir), and more SST-sensitive channels (cf. Kurihara et al. 2016).

MSG SEVIRI. The MSG SEVIRI instrument (Schmetz et al. 2001) sited at 0° longitude provides full-disk observations every 15 min. The resolution of the thermal channels is 3 km at nadir. While the spin–scan nature of the platform means that the imager's noise per pixel is higher than for a three-axis-stabilized platform, it provides the added benefit of a more stable thermal environment for the instrument with concomitant reduction in diurnal calibration variability. One slight complication with the SEVIRI instrument is the spectral response function of the 3.8-μm channel, which is much broader than for the equivalent channels on other imagers, thus leading to a somewhat degraded SST retrieval capability (e.g., Merchant et al. 2009).

Level 2 (L2) SST products. NOAA is in a unique position that every L2 SST dataset used in this product is a geophysical variable derived from level 1 source data at the same resolution and location as the level 1 data (i.e., satellite projection with geographic information). The level 2 SST input dataset is actually processed in house. The radiance data are received directly for sensors that NOAA manages (*SNPP*, GOES-East and -West), or pushed from other operational sources—EUMETSAT for MSG and MetOp, and the BoM for data from MTSAT. The polar-orbiting data are processed using the Advanced Clear Sky Processor for Oceans (ACSPO) system (Petrenko et al. 2010). The exact form of the retrieval algorithm has recently changed from the nonlinear SST (NLSST) form to that chosen by the EUMETSAT Satellite Application Facility on Ocean and Sea Ice (OSI SAF), but is still developed by regression to in situ, so that some regional biases still exist in the product (Petrenko et al. 2014). The full capabilities of the five SST-sensitive VIIRS channels remain to be exploited in the ACSPO product.

The geostationary data are processed using a Bayesian cloud detection methodology (Merchant et al. 2005). The GOES SST product is described in Maturi et al. (2008). The SST products for the other geostationary sensors are processed in a similar manner. The previous retrieval methodology is similar to the OSI SAF formulation (Merchant et al. 2008), which is to be expected since they were primarily developed by the same person. A deterministic physical retrieval methodology was adopted for the geostationary SST processing in August 2013 that demonstrates significantly better results (Koner et al. 2015). The fixed viewing geometry of geostationary imagers with respect to major features of atmospheric and oceanic circulation means that some biases in the retrieved SST field are inevitable. This was particularly true prior to the adoption of the physical deterministic retrieval methodology.

While the SST data are available as single scenes in the L2P format specified by the Group for High Resolution Sea Surface Temperature (GHRSST; Donlon et al. 2007), the geostationary data currently utilized in the operational product are postprocessed into hourly averages on a 1/20° equal-angle grid (Maturi et al. 2008).

Ancillary input data. Before data from multiple sources can be combined, the observations for each piece of data need bias correction relative to each other. Initially, bias corrections used for a day's analysis were derived from the previous day's satellite data and SST analysis, but this method results in a slow drift in the global field. As a result, an independent bias correction reference was selected, and a high-resolution version of the National Centers for Environmental Prediction (NCEP) real-time global (RTG) SST (Thiébaux et al. 2003) was adopted. The high-resolution version 1/12° (9 km) has the additional advantage of using SSTs from AVHRR using

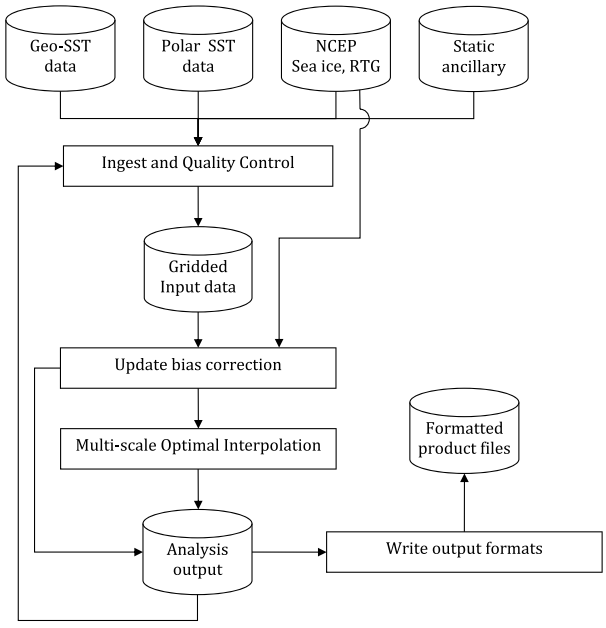

Fig. 1. Process flowchart showing main components.

a physical stochastic retrieval methodology that reduces the regional biases due to local atmospheric conditions (Gemmill et al. 2007). Furthermore, the RTG analysis utilizes in situ data from both moored and drifting buoys to help remove residual biases in its input satellite SST field.

Another source of error is the presence of sea ice. Input data affected by sea ice need to be identified and screened. The NCEP sea ice analysis (Grumbine 2014) is produced daily, again at a grid resolution of 9 km, and is used as an ice mask because it matches the resolution of the high-resolution RTG SST. Obtaining a higher-resolution ice mask on a daily basis is difficult because the implied all-weather requirement dictates the use of passive microwave data of relatively low resolution.

PROCESSING METHODOLOGY. The major steps for generating the Geo-Polar SST analysis are as follows:

- Grid each input data type at the analysis resolution.
- Estimate bias corrections for each of the input grids.
- Perform multiscale optimal interpolation analysis.
- Output result in specified formats for end users.

The above process is illustrated in Fig. 1 with further details.

Input data gridding. The input SST data for each 24-h period (UTC day) are first combined into equal-angle grids at the analysis resolution. Each input source is treated independently in the gridding process. For example, GOES-East daytime data are classified as a single input data type.

Data types. The reason for separation into day and night for individual sensors is that geographic distribution and magnitude of biases and retrieval accuracies for each data type typically differ between day and night and, therefore, are best treated independently. The need for separate treatment of daytime and nighttime biases has long been recognized (e.g., Reynolds and Smith 1994). The fact that such variations exist is not surprising since daytime and nighttime cloud detection schemes are usually different (e.g., Merchant et al. 2005) as are the actual retrieval algorithms (e.g., Merchant et al. 2008; Petrenko et al. 2014). Similarly, surface warming is prevalent during the day, and usually peaks around midafternoon (e.g., Gentemann et al. 2003); thus, polar-orbiting satellites in afternoon orbits experience more diurnal warming than those with equator-crossing times in midmorning. Again, geostationary sensors each have a specific field of view with respect to patterns of atmospheric and oceanic circulation, as well as different cycles of diurnal calibration bias.

Gridding methodology. Gridding the input data provides two main benefits. First, it reduces the volume of data to be analyzed by the estimation scheme. Second, it gives an opportunity to apply particular quality control (QC) procedures to eliminate bad data (e.g., cloud contaminated observations that have not been flagged). Since the input data are biased, they are first adjusted using the bias correction for that data type from the previous day. The QC process itself involves checking the input data against the previous day's analyzed SST combined with an estimate of local variability updated each day, with the anticipated retrieval accuracy for that data type, in order to give a combined threshold for excluding bad data. If there are at least five observations for a particular data type in a grid cell, then an additional standard deviation test is applied to remove data outside 2σ. This test is relevant for high-resolution VIIRS and MetOp SSTs, since many SST values may be available within one grid cell from a single swath, as well as geostationary data where data from multiple images may be combined. The error of the pixels that pass QC for each grid cell is calculated if there are at least three good observations; otherwise, it is specified for the given observation type based on typical validation values with respect to in situ.

Figure 2 shows the relative coverage of geostationary and polar-orbiting satellite sources of SST data for

a single day. For the polar data, there are significant regions of the ocean where persistent cloud cover does not allow good SST observations from infrared instruments, even though each area has been imaged roughly four times. Such regions are substantially reduced for geostationary data, at least where those SST products are available. In particular, regions of "broken" cloud fields in the polar data have been reduced. Unfortunately, some areas have no satellite input for the entire 24-h period, as either cloud or sea ice. To provide some data everywhere (especially in regions of sea ice), the RTG data are included as a separate data type that is not bias corrected and used as a reference. These data are thinned to provide one observation every five grid cells in latitude and longitude. Thus in cloud-free regions the direct contribution of the RTG to the Geo-Polar analysis SST is negligible, as it is overwhelmed by the higher-density contributions from the other input data types. There is a significant advantage in ice-covered regions, since the RTG itself uses the NCEP ice concentration to derive an ocean temperature via Millero's formula and climatological salinity (Thiébaux et al. 2003).

Bias corrections. The bias correction field for each input data type is obtained by first differencing the gridded input SST data from the RTG analysis for the same day. The bias value is a weighted combination of this difference field and the bias field for the previous day and is quite forward weighted (60:40) to allow for rapid updates that occur as a result of passage of atmospheric features affecting regional SST accuracy. If no data exist for a particular input grid cell, the bias value for that data type and location from the previous day is used. The resultant bias correction field is then spatially smoothed over 2° × 2° to preserve the high-resolution features in the input data. If this were not done, the resultant Geo-Polar SST analysis would be almost indistinguishable from the RTG itself. (The impact of preserving the high-resolution information, cf. the RTG, can be gleaned from Fig. 4 below.) The bias corrections for the day in question are subtracted from the gridded observations prior to obtaining the individual anomaly fields, which are then analyzed by the multiscale optimal estimator.

Multiscale optimal estimation. Details of the underlying methodology can be found in Khellah et al. (2005). The method employs a recursive estimation algorithm that emulates a Kalman filter, with a rapid multiscale optimum interpolation (OI) algorithm used for the update step (Fieguth et al. 1998, 2003). This approach preserves the finescale structure in SST

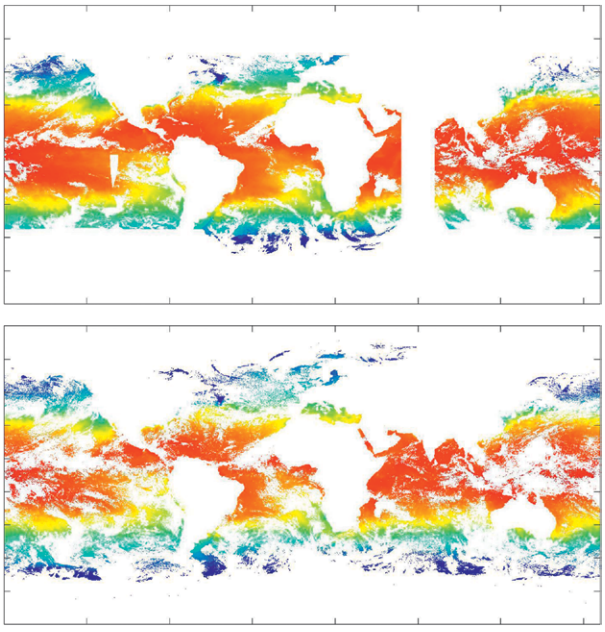

Fig. 2. One day of (top) geostationary SST data and (bottom) polar-orbiting SST data. Where the geostationary data are available (the coverage boundaries are reasonably evident), the data density is higher, as evidenced by the fact that regions for which no observation is available are significantly diminished with respect to the polar-orbiting data.

estimates and allows geophysical realistic treatment of land–sea boundaries. The sequential estimation technique enables observations from different times to contribute appropriately to the SST estimate and to propagate realistic error estimates based on both old and new SST observations. The approach is to divide and conquer: statistics are sought to conditionally decorrelate spatial subsets of observations so that each can be processed independently. In physical terms, this corresponds to assuming that for each subset, the influence of the external SST field can be completely represented by knowledge of the SST around the boundary. Completely sampling the boundary would yield an optimal solution; however, subsampling the boundary achieves a useful approximation and offers a computationally efficient method for interpolation of extremely large datasets.

A prior model that captures the inherent spatial variability of the SST field must be determined. Investigation with model data has demonstrated the necessity of using nonstationary anisotropic models that adapt to the measurement density of the SST observations. This is achieved using a multipass approach in which a range of fixed correlation lengths (1/*e* length scales of 8, 16, and 32 grid cells) are used to generate stationary estimates, which are then interpolated to produce the

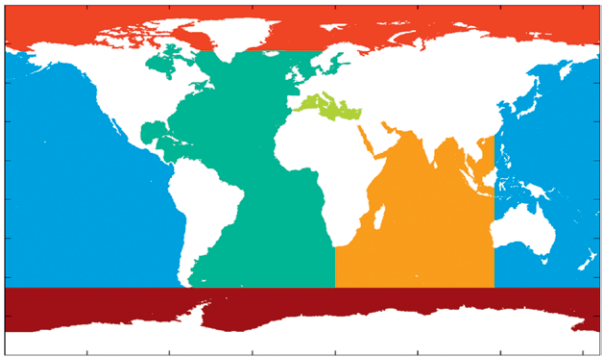

Fig. 3. Delineation of separate ocean basins in SST analysis: Atlantic (teal), Indian (orange), Pacific (blue), Arctic (red), and Southern (brown) Oceans and Mediterranean Sea (green).

desired nonstationary estimates and errors. We use a mixture of stationary models to accurately mimic the effect of a nonstationary prior (again, see Khellah et al. 2005). One benefit of using stationary priors is the ability to preserve mathematical rigor in the OI step. Schemes that use nonstationary priors have to ensure that the correlation lengths change slowly to avoid complications. With our approach, the effective correlation length can change rapidly (assuming there are sufficient data to support it); thus. the interpolation is governed by local data density.

In the prediction step, the system dynamics predict both the new SST estimate and the associated error information. We assume that the ocean dynamics are very slow so that a very simple dynamic model—each pixel independently evolving randomly—is appropriate. This model implies the following simple estimated conditional prediction: $T(t|t-1) = T(t-1|t-1)$; that is, no climatological drift is applied to the previous day's analysis. The prior is modified implicitly by introducing new measurements; that is, we consider the measurement at any time t and temperature T consists of two independent components—namely, the new SST observations and the predicted estimate

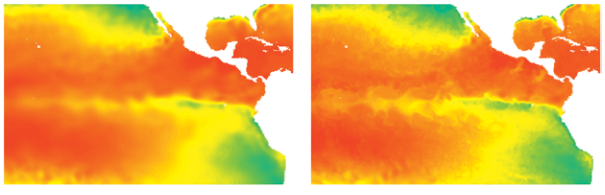

Fig. 4. Comparison of (left) RTG high-resolution 9-km SST analysis and (right) 11-km Geo-Polar SST analysis for 1 Dec 2007. Note the dramatic increase in mesoscale oceanographic detail. The 11-km Geo-Polar SST analysis was initialized using the RTG field for 30 Nov, so the (right) image represents the impact of just 1 day of geostationary data.

from the previous time step. The new SST estimate results from adding the estimated anomaly field to the previous SST estimate. Propagation of error statistics is achieved by appropriately downweighting the impact of the previous SST estimate through increasing the associated error variance and calculating an error estimate based on both this error and the observational error associated with the new observations.

One additional detail of the Geo-Polar SST analysis procedure is the processing of separate ocean basins. This prevents cross-talk between bodies of water that are not geophysically connected, even though their physical separation may be small enough to lie within some of the correlation length scales. For example, data from the Caribbean cannot influence the eastern Pacific across the Isthmus of Panama. The designated basins are shown in Fig. 3, and coupling between input data in various basins is permitted or denied as appropriate.

Output formats. The Geo-Polar SST analysis fields are currently output in two formats. The "CoastWatch HDF" files (CW-HDF) are in HDF-4 format and contain certain attributes and other information that are pertinent to the NOAA CoastWatch Program (http://coastwatch.noaa.gov). They include mapping information and descriptions of various data fields and flags, as well as analysis uncertainty information for every grid point. Data are also written in GHRSST L4 format (see Donlon et al. 2007), which is netCDF-4 and contains an internationally agreed upon set of information for end users. It should be noted that the GHRSST L4 version of the Geo-Polar SST analysis product (http://dx.doi.org/10.5067/GHGPB-4FO02) is significantly smaller than for the equivalent CW-HDF in terms of data volume, which may be a consideration for some users.

OUTPUT EXAMPLES. The panels of Fig. 4 show the Geo-Polar SST analysis fields over the eastern Pacific and Caribbean for 1 December 2007 for the RTG (left) and our new analysis (right). The analysis was initialized from the RTG field for the previous day, which displayed features similar to those shown in the left-hand panel. A vast increase in geophysical detail is immediately apparent for the new product. This result is for the initial version of the Geo-Polar SST analysis at 11-km resolution that preceded the current 5-km version. It should be noted that the native grid resolution of the RTG is actually 9 km—a value that is clearly not representative of its actual resolving power. Similar findings are reported by Reynolds and Chelton (2010). The impact of the resolution difference between the 9-km RTG and

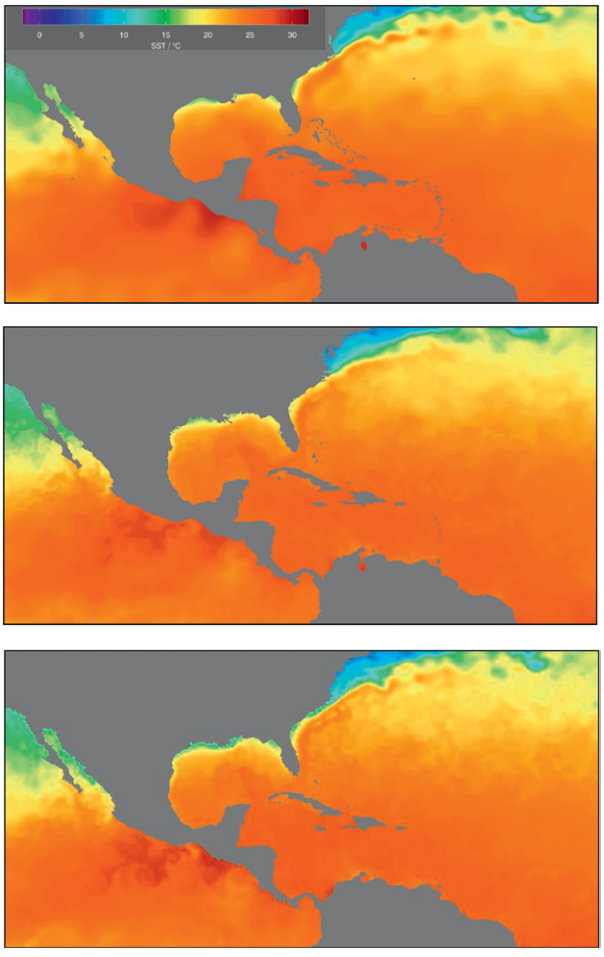

Fig. 5. SST analyses for 31 Dec 2007: (top)–(bottom) 9-km RTG SST analysis, OSTIA 5-km SST reanalysis, and 11-km Geo-Polar SST analysis.

the 5-km Geo-Polar SST analysis is negligible at the scale of the image shown in Fig. 4. Figure 5 again shows the 11-km Geo-Polar SST analysis (this time for 31 December 2007) with the RTG and Ocean Surface Temperature and Ice Analysis (OSTIA; in this case, the reanalysis product, Roberts-Jones et al. 2012) products for comparison. The most remarkable feature is the "split" Gulf Stream, which, as far as we are aware, is not fully reproduced in any SST analysis using only infrared SST data as an input, although there is some suggestion in the OSTIA reanalysis. The characteristic hourglass shape of this short-lived feature can be seen in microwave SST data (Fig. 6). This illustrates the benefit of including data from geostationary sensors in the analysis—the combined effect of 24-h fields, each derived from two individual SST images. This combination is sufficient to allow the analysis to obtain a good, high-resolution estimate of the underlying SST field, even in the presence of heavy wintertime cloud.

While the 11-km Geo-Polar SST analysis was capable of revealing substantial geophysical detail, it was decided to double the grid resolution, thereby halving the minimum correlation length scale. The effect of changing the grid resolution is shown in Fig. 7. It can be seen that the 5-km Geo-Polar SST analysis reveals a lot of mesoscale information that is not quite resolved in the 11-km Geo-Polar SST analysis, including evidence of return eddies along the edge of the Gulf Stream and shallow shelf regions in the vicinity of Abaco, Cuba, and other islands.

PRODUCT ACCURACY. *Ground truth data.* The in situ data used to validate the Geo-Polar SST analysis originate from the World Meteorological Organization's Global Telecommunications System, which broadcasts operational data to a variety of users (principally national meteorological services). These data are initially collected by NCEP and then are subjected to quality control processing via the NESDIS/Center for Satellite Applications and Research (STAR) in situ Quality Monitor (iQuam) system (www.star.nesdis.noaa.gov/sod/sst/iquam/; also see Xu and Ignatov 2014). The data globally distributed number several thousand observations per day. For the purposes of this validation, only quality controlled drifters are considered. The matchup pairs are constructed by choosing daily average values (location and SST) for individual drifters inside each analysis grid cell. The average in situ SST values (in 5° × 5°) boxes for 2014 can be seen in the top panel of Fig. 8. If an L4 analysis includes drifter measurements, then such validation would not be fully independent. It should be noted that in situ data are not ingested directly into our analysis. The bottom panel of Fig. 8 shows that, as expected, standard deviation values are highest in oceanographically active regions (primarily boundary currents).

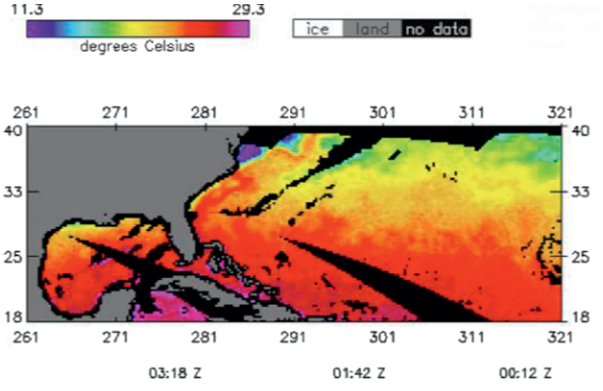

Fig. 6. TRMM Microwave Imager SST for 31 Dec 2007. Note the hourglass pattern in the Gulf Stream. Image courtesy of Remote Sensing Systems.

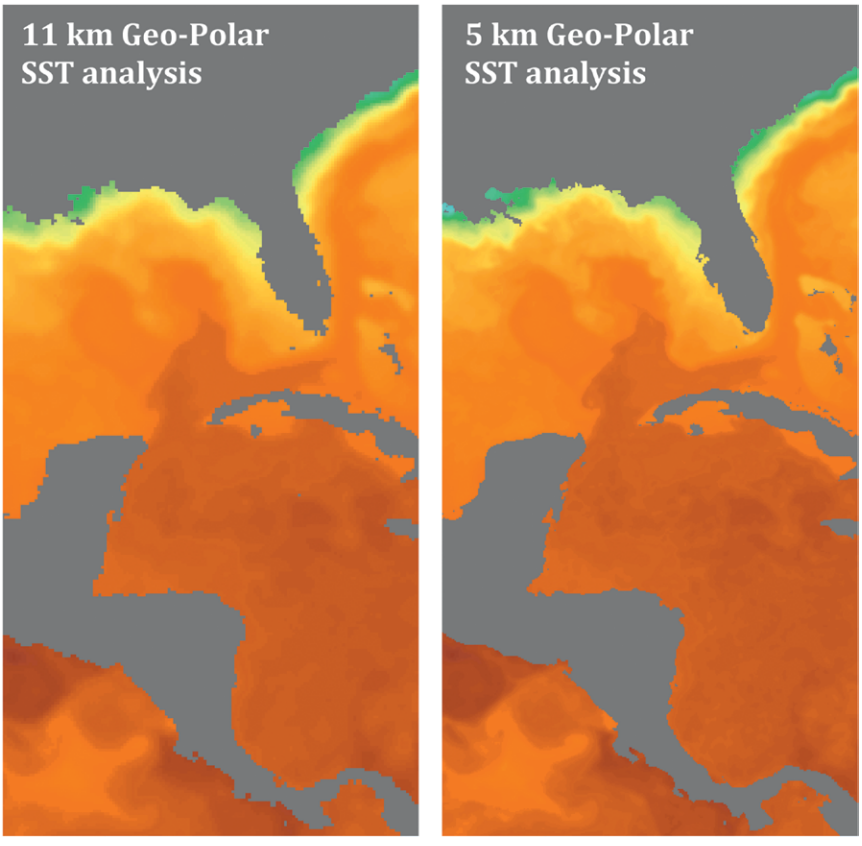

Fig. 7. The Caribbean, Gulf Loop Current, and Gulf Stream are shown for the (left) 11-km Geo-Polar SST analysis and (right) 5-km Geo-Polar SST analysis.

Performance estimates. The time series of results obtained from the matchup differences of the Geo-Polar SST analysis against drifter data for the period May 2012–August 2015 can be seen in Fig. 9. For comparison purposes, while transitioning from the 11-km Geo-Polar SST analysis to the 5-km Geo-Polar SST analysis, statistical time series of the 11-km Geo-Polar SST analysis are also overlaid. The robust standard deviation (RSD) is consistently at or below a value of 0.3 K for the time series, at least since October 2013, and is always less than the previous 11-km Geo-Polar SST analysis. The RSD is the equivalent standard deviation for a Gaussian that has the same interquartile range and is much more representative of the main peak of the data (Merchant and Harris 1999). A physical deterministic retrieval was implemented operationally for our geostationary SST product in August 2013, although postprocessing issues meant that these data were not flowing correctly to the SST analysis until September 2013. The improved accuracy of the geostationary inputs may be one reason for the better performance of the SST analysis from October 2013. A recent rise in standard deviation above its typical value of ≤0.4 K peaks around July 2015, and likely can be traced back to increased error in the input data, particularly for the polar orbiter SSTs (Fig. 10). In any case, a steady improvement in product accuracy is observed from year to year, particularly when considering the robust standard deviation value. There is also a noticeable improvement in accuracy for the 5-km Geo-Polar SST analysis compared to the original 11-km Geo-Polar SST analysis. Ongoing validation information is available at www.star.nesdis.noaa.gov/sod/sst/squam/L4/. The web page shows results for a substantial number of other GHRSST-format L4 analyses compared to in situ data. Since some analyses ingest in situ data in their production, such comparisons need to be treated accordingly (Dash et al. 2012). Preservation of genuine small-scale geophysical variability while avoiding increased noise is a key goal of the product, but a quantified assessment of these qualities will require detailed analysis similar to that reported in Reynolds and Chelton (2010). Their assessment of the OSTIA analysis is favorable in terms of high-frequency information, and a relative comparison to our product is facilitated by Fig. 5.

APPLICATIONS OF THE GEO-POLAR SST ANALYSIS. The new analysis has been developed to meet the needs of both the national and international user communities. These include 1) the National Weather Service ocean model forecasting, 2) CoastWatch/OceanWatch mesoscale oceanography, 3) NOAA Coral Reef Watch bleaching alerts, 3) National Marine Fisheries Service management of fisheries and mammals, 4) the National Hurricane Center and the National Weather Service offices oceanic heat content (OHC) products, and 5) the international users represented by the GHRSST community.

Ocean model forecasting. One of NCEP's Environmental Modeling Center's primary concerns is accurate mesoscale forecasting during the East Coast winter storm

season. The Geo-Polar SST analysis is used to validate the SSTs incorporated into the models. In particular, the analysis is used to validate the Real Time Ocean Forecast System (RTOFS) for the North Atlantic. This shows good agreement between the sea surface temperatures generated from the RTOFS North Atlantic and the 5-km Geo-Polar SST analysis.

Mesoscale oceanography. Many CoastWatch/OceanWatch users need mesoscale delineation in the SST products. This product provides a gap-free SST analysis with mesoscale delineation of features. The benefits have been particularly well realized by the Geo-Polar SST analysis since its true resolving power is comparable to the Rossby radius of deformation at midlatitudes, at least where the data density is sufficient to support the minimum correlation length. This ability is evident in Fig. 7, where mesoscale features discerned in the 11-km Geo-Polar SST analysis are substantially sharper in the 5-km Geo-Polar SST analysis.

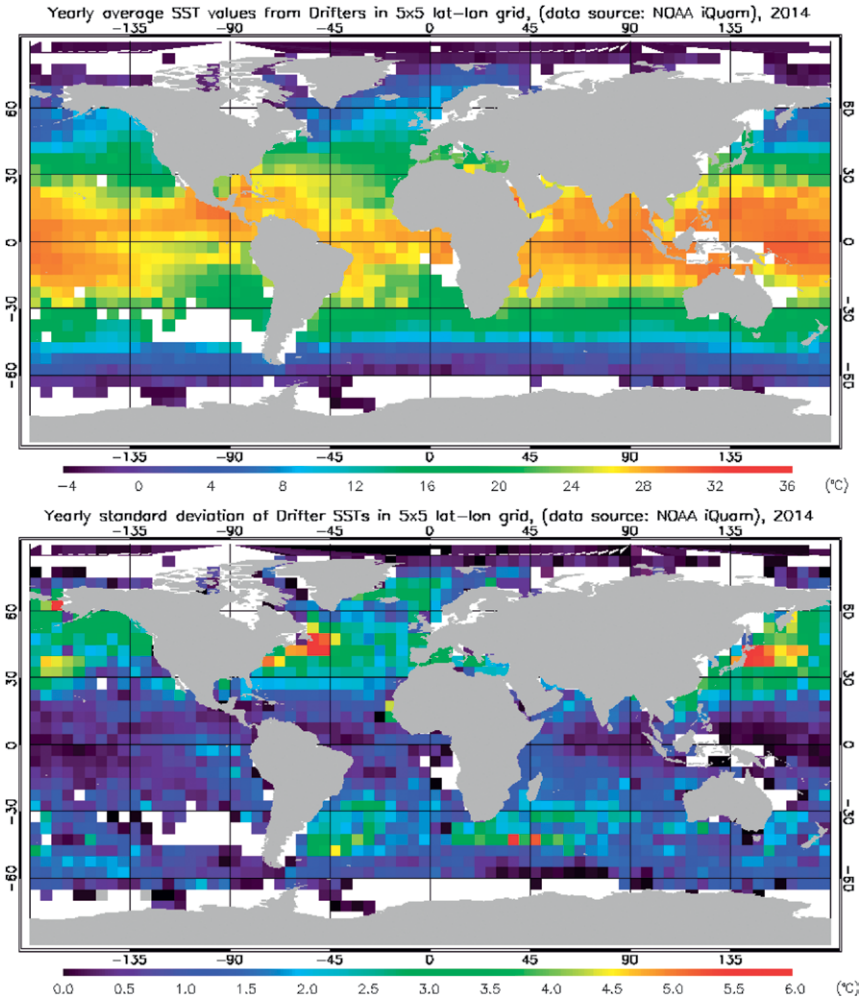

Fig. 8. (top) Mean SST per 5° × 5° box for in situ data from *i*Quam database for 2014. (bottom) The corresponding standard deviation values.

Coral reef watch. The coral reef community needs accurate SSTs and adjustment for diurnal variation. The multiscale aspect of the assimilation methodology permits enhanced local resolution for areas of interest such as coral reefs and remains within a fully consistent global analysis (Liu et al. 2015).

National Marine Fisheries Service (NMFS). The National Marine Fisheries Service is an important user of SSTs for the entire U.S. coastal region in particular fisheries studies related to commercial fisheries management and protection of endangered species. This service includes coral reef marine debris projects, turtle exclusion for fishing, and mammal protection.

The Hawaiin and the Northeast NMFS centers have a government mandate through the Marine Mammal Protection Act, the Endangered Species Act, and the Fur Seal Act along with the Sustainable Fisheries Act. These acts require both the Hawaiian and the Northeast Fisheries Offices to monitor the health and the continuation of these species.

The 5-km Geo-Polar SST analysis is a proven monitoring tool for managing and maintaining the health and life cycles of the above-mentioned species.

NHC and NWS offices. In the present model, the OHC estimates are calculated from our 5-km Geo-Polar SST analysis, combined with *Jason-2,* Satellite with Argos and Altika (SARAL), and *CryoSat-2* altimeter estimates of the 20° and 26°C isotherm depths. The altimeter estimates are derived from a scheme using daily ocean climatology of mean isotherm depths and reduced gravities. OHC products are being generated for the National Hurricane Center (NHC) and National Weather Service (NWS) offices for hurricane intensity forecasting. NESDIS is generating a North

Atlantic OHC product suite (Meyers et al. 2014) for the NHC. A North Pacific and South Pacific OHC product suite (Shay and Brewster 2010) is being generated for the NWS Pacific Region Forecast office. In addition, the Coral Reef Watch uses the OHC product suite to access the heat content for deep-water coral reefs.

GHRSST. GHRSST national and international users are supported by the 5-km Geo-Polar SST analysis, which minimizes the effect of the diurnal cycle and makes optimal use of both polar and geostationary sensors. As previously mentioned, the data provided in GHRSST L4 format are available through the NASA Physical Oceanography Distributed Active Archive Center (PO.DAAC), which serves as the primary user portal for GHRSST products (https://podaac.jpl.nasa.gov/GHRSST).

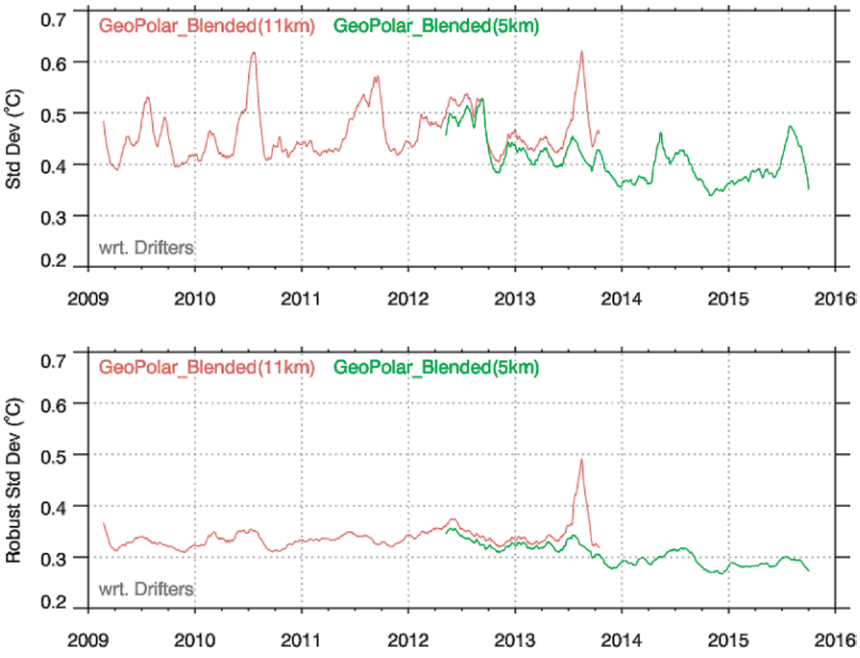

Fig. 9. Time series of validation results for 11-km Geo-Polar SST analysis [GeoPolar_Blended (11 km)] and 5-km Geo-Polar SST analysis [GeoPolar_Blended (5 km)] against *i*Quam quality-controlled buoy data. (top) Standard deviation; (bottom) robust standard deviation statistic.

FUTURE ENHANCEMENTS. Forthcoming enhancements include the incorporation of 1) microwave SST products from the *Global Change Observation Mission for Water-1* (*GCOM-W1*) AMSR-2 instrument to improve the resolution of SST features in areas of persistent cloud, 2) explicit correction for diurnal effects via a turbulence model of upper-ocean heating, and 3) use of the *Sentinel-3* SLSTR-SST for improving the bias corrections of individual data types used in the Geo-Polar SST analysis. In addition, the analysis will continue to benefit from improved input data from new sensors (e.g., the Advanced Baseline Imager on the recently launched *GOES-16* platform), which will be of higher quality and resolution, thus allowing for more effective quality control.

Future products include regional Geo-Polar SST analyses at ~1 km for specified regions for Coral Reef Watch users and NWS ocean forecast models.

SUMMARY. NESDIS has implemented a dynamic data-fusion scheme to generate a global operational sea surface temperature (SST) analysis from polar-orbiting and geostationary SST data. This scheme is based on an optimal interpolation assimilation technique combining multisatellite Geo-Polar SST retrievals into a single analysis of SST at a grid resolution of 5 km, crossing a useful threshold in actual resolving power for many mesoscale oceanographic applications. This analysis deals with the impact of the geostationary

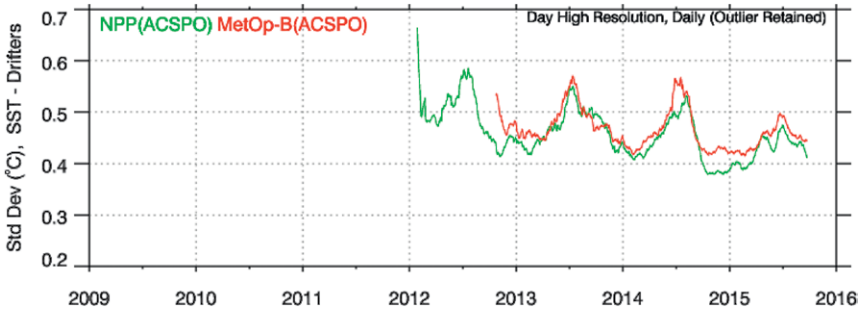

Fig. 10. Time series validation results for daytime ACSPO SSTs from *SNPP* VIIRS (green) and *MetOp-B* AVHRR (red) against *i*Quam quality-controlled buoy data. Note the significant increase in error peaking around Jul each year.

data on coverage and demonstrates the power of the data-adaptive correlation length scale to strike a balance between preserving oceanographic details and reducing noise.

Currently, the 5-km Geo-Polar SST analysis performs well compared to other global high-resolution analyses, particularly with respect to the preservation of high-resolution features without introducing excessive noise. As noted above, this quality is not available from traditional validation approaches of the type reported in Dash et al. (2012). Reports from end users confirm the suitability of our analysis for their applications compared to other products provided on similar grid spacings. The 5-km Geo-Polar SST analysis product is featured on the NESDIS website and in the Smithsonian Ocean Hall exhibit.

ACKNOWLEDGMENTS. This study was supported by NESDIS Product Systems Development Implementation program funds. This study was partially supported by NOAA Grant NA14NES4320003 [Cooperative Institute for Climate and Satellites (CICS)] at the University of Maryland/ESSIC. We thank members of the NOAA Coral Reef Watch team for helpful discussions. The views, opinions, and findings contained in this paper are those of the authors and should not be construed as an official NOAA or U.S. government position, policy, or decision.

REFERENCES

Dash, P., and Coauthors, 2012: Group for High Resolution Sea Surface Temperature (GHRSST) analysis fields inter-comparisons—Part 2: Near real time web-based level 4 SST Quality Monitor (L4-SQUAM). *Deep-Sea Res. II*, **77–80**, 31–43, doi:10.1016/j.dsr2.2012.04.002.

Donlon, C., and Coauthors, 2007: The Global Ocean Data Assimilation Experiment High-Resolution Sea Surface Temperature Pilot Project. *Bull. Amer. Meteor. Soc.*, **88**, 1197–1213, doi:10.1175/BAMS-88-8-1197.

Fieguth, P., D. Menemenlis, T. Ho, A. Willsky, and C. Wunsch, 1998: Mapping Mediterranean altimeter data with a multiresolution optimal interpolation algorithm. *J. Atmos. Oceanic Technol.*, **15**, 535–546, doi:10.1175/1520-0426(1998)015<0535:MMADWA>2.0.CO;2.

——, ——, and I. Fukumori, 2003: Mapping and pseudo-inverse algorithms for ocean data assimilation. *IEEE Trans. Geosci. Remote Sens.*, **41**, 43–51, doi:10.1109/TGRS.2002.808058.

Gemmill, W., B. Katz, and X. Li, 2007: Daily real-time, global sea surface temperature—High-resolution analysis: RTG_SST_HR. NOAA/NWS/NCEP/EMC/MMAB, Science Application International Corporation, and Joint Center for Satellite Data Assimilation Tech. Note 260, 22 pp. [Available online at http://polar.ncep.noaa.gov/mmab/papers/tn260/MMAB260.pdf.]

Gentemann, C. L., C. J. Donlon, A. Stuart-Menteth, and F. J. Wentz, 2003: Diurnal signals in satellite sea surface temperature measurements. *Geophys. Res. Lett.*, **30**, 1140, doi:10.1029/2002GL016291.

Grumbine, R. W., 2014: Automated sea ice concentration analysis history at NCEP 1996-2012. MMAB Tech. Note 321, 39 pp. [Available online at http://polar.ncep.noaa.gov/mmab/papers/tn321/MMAB_321.pdf.]

Harris, A., and E. Maturi, 2003: Assimilation of satellite sea surface temperature retrievals. *Bull. Amer. Meteor. Soc.*, **84**, 1575–1580, doi:10.1175/BAMS-84-11-1575.

Khellah, F., P. W. Fieguth, M. J. Murray, and M. R. Allen, 2005: Statistical processing of large image sequences. *IEEE Trans. Image Process.*, **14**, 80–93, doi:10.1109/TIP.2004.838703.

Koner, P. K., A. Harris, and E. Maturi, 2015: A physical deterministic inverse method for operational satellite remote sensing: An application for sea surface temperature retrievals. *IEEE Trans. Geosci. Remote Sens.*, **53**, 5872–5888, doi:10.1109/TGRS.2015.2424219.

Kurihara, Y., H. Murakami, and M. Kachi, 2016: Sea surface temperature from the new Japanese geostationary meteorological Himawari-8 satellite. *Geophys. Res. Lett.*, **43**, 1234–1240, doi:10.1002/2015GL067159.

Liu, G., and Coauthors, 2014: Reef-scale thermal stress monitoring of coral ecosystems: New 5-km global products from NOAA Coral Reef Watch. *Remote Sens.*, **6**, 11 579–11 606, doi:10.3390/rs61111579.

Martin, M., and Coauthors, 2012: Group for High Resolution Sea Surface temperature (GHRSST) analysis fields inter-comparisons. Part 1: A GHRSST multi-product ensemble (GMPE). *Deep-Sea Res. II*, **77–80**, 21–30, doi:10.1016/j.dsr2.2012.04.013.

Maturi, E., A. Harris, J. Mittaz, C. Merchant, B. Potash, W. Meng, J. Sapper, 2008: NOAA's sea surface products from operational geostationary satellites. *Bull. Amer. Meteor. Soc.*, **89**, 1877–1888, doi:10.1175/2008BAMS2528.1.

Merchant, C. J., and A. R. Harris, 1999: Toward the elimination of bias in satellite retrievals of sea surface temperature: 2. Comparison with in situ measurements. *J. Geophys. Res.*, **104**, 23 579–23 590, doi:10.1029/1999JC900106.

——, ——, E. Maturi, and S. Maccallum, 2005: Probabilistic physically based cloud screening of satellite infrared imagery for operational sea surface temperature retrieval. *Quart. J. Roy. Meteor. Soc.*, **131**, 2735–2755, doi:10.1256/qj.05.15.

——, P. Le Borgne, A. Marsouin, and H. Roquet, 2008: Optimal estimation of sea surface temperature from split-window observations. *Remote Sens. Environ.*, **112**, 2469–2484, doi:10.1016/j.rse.2007.11.011.

——, ——, ——, O. Embury, S. N. MacCallum, J. Mittaz, and C. P. Old, 2009: Sea surface temperature estimation from the *Geostationary Operational Environmental Satellite-12* (*GOES-12*). *J. Atmos. Oceanic Technol.*, **26**, 570–581, doi:10.1175/2008JTECHO596.1.

——, and Coauthors, 2013: The surface temperatures of Earth: Steps towards integrated understanding of variability and change. *Geosci. Instrum. Method. Data Syst.*, **2**, 305–321, doi:10.5194/gi-2-305-2013.

Meyers, P. C., L. K. Shay, and J. K. Brewster, 2014: The development of the systematically merged Atlantic regional temperature and salinity climatology for hurricane intensity forecasting. *J. Atmos. Oceanic Technol.*, **31**, 131–149, doi:10.1175/JTECH-D-13-00100.1.

Mittaz, J., M. Bali, and A. Harris, 2013: The calibration of broad band infrared sensors: Time variable biases and other issues. *2013 Meteorological Satellite Conf.*, Vienna, Austria, EUMETSAT. [Available online at www.eumetsat.int/website/wcm/idc/idcplg?IdcService=GET_FILE&dDocName=PDF_CONF_P_S8_11_MITTAZ_V&RevisionSelectionMethod=LatestReleased&Rendition=Web.]

Petrenko, B., A. Ignatov, Y. Kihai, and A. Heidinger, 2010: Clear-sky mask for the Advanced Clear-Sky Processor for Oceans. *J. Atmos. Oceanic Technol.*, **27**, 1609–1623, doi:10.1175/2010JTECHA1413.1.

——, ——, ——, J. Stroup, and P. Dash, 2014: Evaluation and selection of SST regression algorithms for JPSS VIIRS. *J. Geophys. Res. Atmos.*, **119**, 4580–4599, doi:10.1002/2013JD020637.

Reynolds, R. W, and T. M. Smith, 1994: Improved global sea surface temperature analyses using optimal interpolation. *J. Climate*, **7**, 929–948, doi:10.1175/1520-0442(1994)007<0929:IGSSTA>2.0.CO;2.

——, and D. B. Chelton, 2010: Comparisons of daily sea surface temperature analyses for 2007–08. *J. Climate*, **23**, 3545–3562, doi:10.1175/2010JCLI3294.1.

——, T. M. Smith, C. Liu, D. B. Chelton, K. S. Casey, and M. G. Schlax, 2007: Daily high-resolution-blended analyses for sea surface temperature. *J. Climate*, **20**, 5473–5496, doi:10.1175/2007JCLI1824.1.

Roberts-Jones, J., E. K. Fiedler, and M. J. Martin, 2012: Daily, global, high-resolution SST and sea ice reanalysis for 1985–2007 using the OSTIA system. *J. Climate*, **25**, 6215–6232, doi:10.1175/JCLI-D-11-00648.1.

Schmetz, J., P. Pili, A. Ratier, S. Rota, and S. Tjemkes, 2001: METEOSAT Second Generation (MSG): Capabilities and applications. *Proc. 11th Conf. on Satellite Meteorology and Oceanography*, Madison, WI, Amer. Meteor. Soc., 6.5. [Available online at https://ams.confex.com/ams/11satellite/techprogram/paper_23827.htm.]

Shay, L. K., and J. Brewster, 2010: Oceanic heat content variability in the eastern Pacific Ocean for hurricane intensity forecasting. *Mon. Wea. Rev.*, **138**, 2110–2131, doi:10.1175/2010MWR3189.1.

Thiébaux, J., E. Rogers, W. Wang, and B. Katz, 2003: A new high-resolution blended real-time global sea surface temperature analysis. *Bull. Amer. Meteor. Soc.*, **84**, 645–656, doi:10.1175/BAMS-84-5-645.

Xu, F., and A. Ignatov, 2014: In situ SST Quality Monitor (*i*Quam). *J. Atmos. Oceanic Technol.*, **31**, 164–180, doi:10.1175/JTECH-D-13-00121.1.

Yu, F., X. Wu, M. K. Rama Varma Raja, Y. Li, L. Wang, and M. Goldberg, 2013: Evaluations of diurnal calibration variation and scan angle emissivity calibration for GOES Imager infrared channels. *IEEE Trans. Geosci. Remote Sens.*, **51**, 671–683, doi:10.1109/TGRS.2012.2197627.